Korean J. Chem. Eng., 35(4), 1019-1025 (2018)
DOI: 10.1007/s11814-017-0355-z

pISSN: 0256-1115
eISSN: 1975-7220

Hydrothermally synthesized highly dispersed $Na_2Ti_3O_7$ nanotubes and their photocatalytic degradation and H_2 evolution activity under UV and simulated solar light irradiation

S. V. Prabhakar Vattikuti*,†, Police Anil Kumar Reddy, Narendra Bandaru***, Jaesool Shim*,†, and Chan Byon****

*School of Mechanical Engineering, Yeungnam University, Gyeongsan 38541, Korea
**School of Mechanical and Nuclear Engineering, Ulsan National Institute of Science and Technology (UNIST), Ulsan 44919, Korea
***Department of Material Science and Engineering, IIT Gandhi Nagar, Ahmedabad, India
(*Received 26 September 2017 • accepted 26 December 2017*)

Abstract−Photocatalytic water splitting technologies are currently being considered for alternative energy sources. However, the strong demand for a high H_2 production rate will present conflicting requirements of excellent photoactivity and low-cost photocatalysts. The first alternative may be abundant nanostructured titanate-related materials as a photocatalyst. Here, we report highly dispersed $Na_2Ti_3O_7$ nanotubes synthesized via a facile hydrothermal route for photocatalytic degradation of Rhodamine B (RhB) and the water splitting under UV-visible light irradiation. Compared with commercial TiO_2, the nanostructured $Na_2Ti_3O_7$ demonstrated excellent photodegradation and water splitting performance, thus addressing the need for low-cost photocatalysts. The as-synthesized $Na_2Ti_3O_7$ nanotubes exhibited desirable photodegradation, and rate of H_2 production was 1,755 $\mu mol \cdot g^{-1} \cdot h^{-1}$ and 1,130 $\mu mol \cdot g^{-1} \cdot h^{-1}$ under UV and simulated solar light irradiation, respectively; the resulting as-synthesized $Na_2Ti_3O_7$ nanotubes are active in UV light than that of visible light response.

Keywords: Photocatalysts, $Na_2Ti_3O_7$, Hydrogen Evolution, Pollutants, Renewable Energy

INTRODUCTION

The use of low-cost nanostructured photocatalyst to degrade pollutants and generate hydrogen has the potential to meet global demand for environmental remediation and the production of clean energy. Many studies are currently focused on the use of various nanostructured alkali metal titanates with the general formula of $A_2Ti_nO_{2n+1}$ (n=3 or 8, and A=Na, Li, K), and various titanate nanostructures have been developed, including nanosheets [1], nanopellets [2], nanoribbons [3], and nanotubes [3,4], which exhibit distinct advantages over commercial TiO_2. In addition, researchers have demonstrated the use of these nanostructures for a wide range of applications, including sodium-ion batteries [5,6], acidic catalytic activity [7], fuel cell electrolytes [8], sensors [9] and electrochemical cell [10]. However, studies on highly dispersed nanotube structures on their applications in photocatalysis and water splitting have rarely been reported involving the fabrication of low-cost photocatalysts or revealing their potential applications as very effective photocatalysts.

$Na_2Ti_3O_7$-based photocatalysts are commonly adopted for fundamental studies due to their low cost, abundant precursors, and easy preparation [2,4,11]. In addition, with its progressive intrinsic properties including variable and tunable conduction/valence band energies, band gaps, and specific surface areas, $Na_2Ti_3O_7$ has been extensively investigated for the photodegradation of pollutants. However, $Na_2Ti_3O_7$ is less active for the photocatalytic production of hydrogen under visible light. $Na_2Ti_3O_7$ is conventionally prepared via solid-state reactions followed by annealing at high temperatures (800-850 °C), as reported by Izawa et al. [12]. However, conventional solid-state synthesis has a few drawbacks: it requires high sintering temperatures, and inevitably results in the non-uniform fabrication of coarse particles due to the volatile nature of the alkaline constituent at evaluated temperatures [1]. Zhang et al. [13] reported hydrothermally synthesized $Na_2Ti_3O_7$ micro-to-nanotubes that exhibited excellent storage performance with a long cycling life. Therefore, a systematic synthesis process is required, and selecting a suitable route for the large-scale fabrication of nanostructured titanate materials remains a great challenge. Meanwhile, hydrothermal reactions have been employed to prepare ultrafine and uniform nanostructures with high purity in a single step without using expensive reagents [14]. However, photocatalytic water splitting with highly dispersed $Na_2Ti_3O_7$ nanotubes has not been reported in the literature thus far.

The aim of the present work was to enhance the single-step hydrothermal method to prepare pure-phase $Na_2Ti_3O_7$ and to study its photocatalytic performance for the degradation of rhodamine B (RhB) as a model pollutant and for the production of hydrogen by water splitting. The synthetic procedure is a low-cost, one-step reaction that requires neither a special experimental setup nor special chemicals. In addition, we investigated its photocatalytic mechanism, which is enhanced by its fast charge transfer, as proven by its excellent electrochemical response along with its impressive cycling

†To whom correspondence should be addressed.
E-mail: vsvprabu@gmail.com, jshim@ynu.ac.kr

performance. We also report for the first time a stimulating phenomenon related to the appearance of a new charge plateau with a potential of 0-0.6 V. Furthermore, cyclic voltammetry (CV) and electrochemical impedance spectroscopy (EIS) were performed on $Na_2Ti_3O_7$ to understand the charge transfer kinetics within the $Na_2Ti_3O_7$ nanotube electrode. Our results demonstrated that the $Na_2Ti_3O_7$ nanotube photocatalyst is a promising candidate electrode material for photoelectrochemical cell applications.

EXPERIMENTAL

1. Synthesis

Hydrothermal methods are the most economical and successful methods for synthesizing metal oxides, especially titanate-based materials. Therefore, $Na_2Ti_3O_7$ titanate nanotubes were prepared by a hydrothermal method using TiO_2 (P25) as the starting material. In a typical synthesis procedure, 2.0 g of TiO_2 was dispersed in 160 mL of a 10 M NaOH aqueous solution, transferred into a Teflon-lined autoclave (250 mL capacity), and heated in an oven at 130 °C for 20 h. The white precipitate was collected and washed with deionized water and ethanol and then dried at 100 °C for 2 h.

2. Characterization

The elemental compositions of the samples were confirmed via energy dispersive X-ray spectroscopy (EDAX). The X-ray diffraction patterns of the samples were recorded (Seifert 3003 TT X-ray diffractometer with 1.5406 Å Cu-Kα radiation) to analyze their phase purities and crystal structures. The morphologies and crystallite sizes of the samples were analyzed via field emission scanning electron microscopy (FESEM, HITACHI S-4200) and transmission electron microscopy (TEM, FEI Tecnai-12). Raman spectra were recorded using a Nicolet 6700 (Thermo Fisher Scientific) with a 532-nm laser source. Diffuse reflectance spectroscopy (DRS, Cary 5000) measurements were recorded using an UV-vis-near-infrared (NIR) double-beam spectrophotometer. N_2 adsorption-desorption isotherms were recorded using a Micromeritics ASAP 2420 surface area analyzer at the temperature of liquid N_2. Before gas adsorption, the sample was degassed at 200 °C for 1 h.

3. Photocatalytic Degradation and H_2 Evolution Studies

The photocatalytic degradation of RhB was under UV irradiation with a 4 W UV lamp with a wavelength of 254 nm. First, 100 mg of the $Na_2Ti_3O_7$ nanotube catalysts and 100 mL of the RhB solution were mixed in a reactor. This solution was stirred at 20 °C in the dark for 60 min to equilibrate the mixture, and then, 5 mL of the reaction mixture was collected every 5 min with a syringe and immediately centrifuged to discover the effect of RhB adsorption on the catalyst. After the UV lamp was turned on, 4 mL of the reaction mixture was collected at 5 min intervals. The collected solutions were analyzed with a UV-vis-NIR Cary 500 spectrophotometer.

The photocatalytic hydrogen evolution reaction (HER) was carried out via water splitting under both of UV light (8 W lamp, wavelength of 365 nm) and simulated solar light irradiation (i.e., a light intensity of 100 mW·cm^{-2}). 5 mg of the catalyst was added to 50 mL of a 5% aqueous glycerol solution in a 150-mL quartz reactor with a long neck, which was then sealed with an air-tight rubber septum and stirred at 500 rpm for 30 min. Then, the reactor was evacuated for 30 min, and the solution was purged with N_2 gas for another 60 min. The amount of H_2 gas produced during the course of the reaction was monitored at hourly intervals by extracting gas samples through the rubber septum using an airtight syringe. The samples were analyzed by gas chromatograph (Shimadzu GC-2014) equipped with a TCD detector and a molecular sieve 5A column with N_2 as the carrier gas.

4. Electrochemical Studies

Photoelectrochemical measurements including linear sweep voltammetry (LSV) and Electron impedance spectroscopy (EIS) involved a three-electrode system using a Biologic SP200 electrochemical workstation. The reference and counter electrodes were Ag/AgCl (in saturated KCl) and a platinum wire, respectively, and a 0.5 M Na_2S aqueous solution served as the electrolyte. To prepare the working electrode, 10 mg of the as-synthesized $Na_2Ti_3O_7$ nanotubes was first dispersed in 450 μL of ethanol with 50 μL of a Nafion mixture using soft ultrasonic stirring to obtain a uniform gel suspension. The solution containing the catalyst (30 μL) was dropped onto a pretreated indium-tin oxide (ITO) conductor glass substrate, which was then dried in an oven at 95 °C for 2 h.

RESULTS AND DISCUSSION

Fig. 1(a) shows the XRD pattern of the commercial TiO_2 (P25) and $Na_2Ti_3O_7$ nanotubes. The P25 TiO_2 is a mixture of 80% anatase and 20% rutile phases and accordingly it showed (101), (004), (200), (105), (211), (204), (116), (220), (215) peaks for anatase and (110), (101), (111) planes for rutile crystallites. Whereas, $Na_2Ti_3O_7$ nanotubes mainly exhibited six broad peaks at 2θ values of 10.53°, 25.61°, 29.69°, 43.92°, 49.03°, and 62.93° corresponding to the (001), (011), (301), (401), (021), and (205) planes, respectively. In addition, all major diffraction peaks could be indexed to monoclinic $Na_2Ti_3O_7$ with lattice constants of a=9.128 Å and c=8.561 Å, which are in agreement with the standard values (JCPDS card No. 31-1329) and are consistent with the results reported in the literature [6]. No additional characteristic diffraction peaks were observed, which indicates that pure $Na_2Ti_3O_7$ was obtained and the $Na_2Ti_3O_7$ with three TiO_6 octahedra in a unit cell has a tubular structure, as shown in the inset of Fig. 1(a). The SEM images in Fig. 1(b), (c) demonstrate the morphology of randomly distributed $Na_2Ti_3O_7$, presenting tube-like nanostructure with lengths of a few tens of nanometers to micrometers. Fig. 1(d) shows the one-dimensional (1D), highly dispersed mesoporous structure of the $Na_2Ti_3O_7$ nanotubes with few nanometers in diameter. The SAED pattern, inset in Fig. 1(d), reveals that the $Na_2Ti_3O_7$ nanotubes are partially-crystalline. The exposed edges of $Na_2Ti_3O_7$ nanotubes can offer more active sites for the HER.

Fig. 2(a) shows the Raman spectra of TiO_2 (P25) and the as-synthesized $Na_2Ti_3O_7$ nanotubes. The P25 TiO_2 displayed characteristic vibrational bands around 141.5 cm^{-1} (E_g), 195.1 cm^{-1} (E_g), 395.4 cm^{-1} (B_{1g}), 512.7 cm^{-1} (A_{1g}) and 635.7 cm^{-1} (E_g) attributed to anatase phase of TiO_2 which were confirmed from the XRD results. The Raman spectrum of the as-prepared $Na_2Ti_3O_7$ exhibited strong peaks at 268, 438 and 650 cm^{-1}, wherein the first peak is ascribed to the Na-O-Ti stretching mode, and the middle peak at 438 cm^{-1} can be assigned to the bending mode of framework Ti-O for the

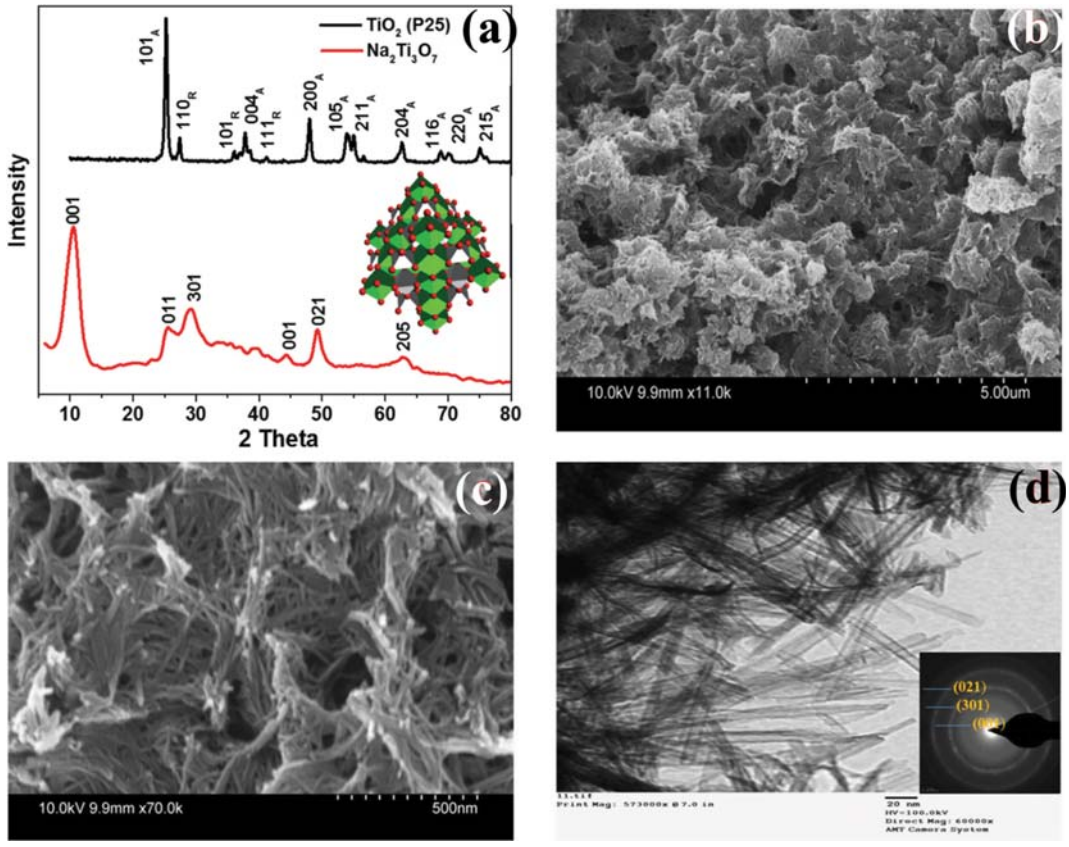

Fig. 1. (a) XRD pattern of TiO2 (P25) and as-prepared $Na_2Ti_3O_7$ nanotubes, (b), (c) SEM images and (d) HRTEM images of as-prepared $Na_2Ti_3O_7$ nanotubes.

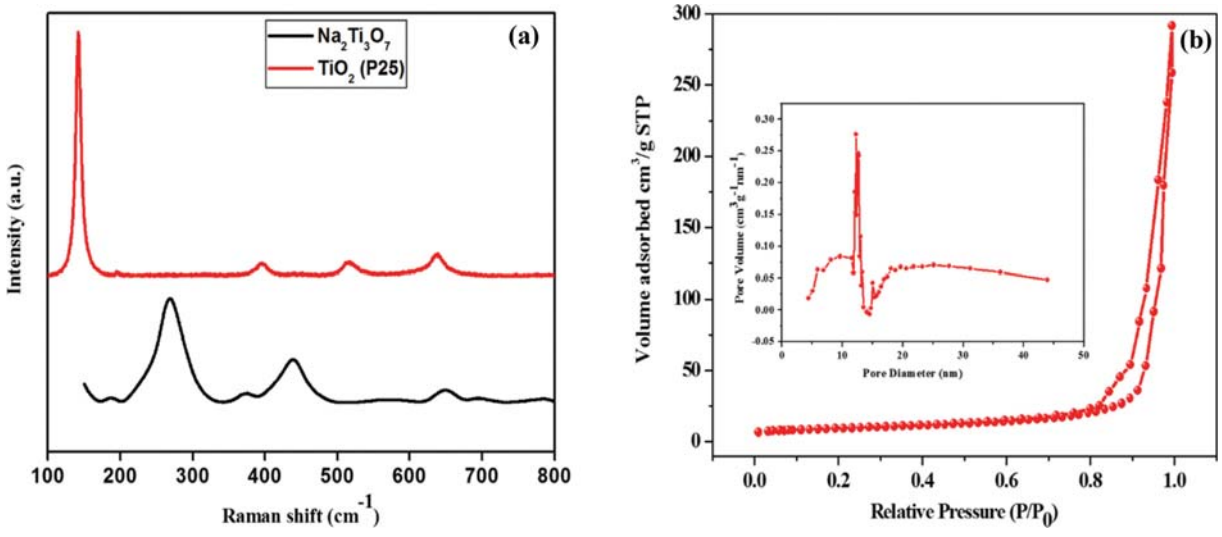

Fig. 2. (a) Raman spectra of as-prepared $Na_2Ti_3O_7$ nanotubes and TiO_2 (P25) and (b) N_2 adsorption/desorption isotherm, inset: Pore size distribution of $Na_2Ti_3O_7$ nanotubes.

three-fold oxygen. Another peak at 650 cm^{-1} is assigned to Ti-O-Ti stretching in edge-sharing TiO_6 [15]. The specific surface area and mesoporous structure of as-prepared $Na_2Ti_3O_7$ were estimated using liquid nitrogen (N_2) adsorption-desorption isotherms, as shown in Fig. 2(b). The sample was degassed at 498 K under vacuum at 10^{-3} Torr for 6 h prior to measurement. The adsorption of N_2 considerably increased above P/P_0~0.8, which was ascribed to capillary condensation followed by a type IV isotherm. Using the Brunauer-Emmett-Teller (BET) equation, the specific surface area of the as-prepared $Na_2Ti_3O_7$ nanotubes was estimated

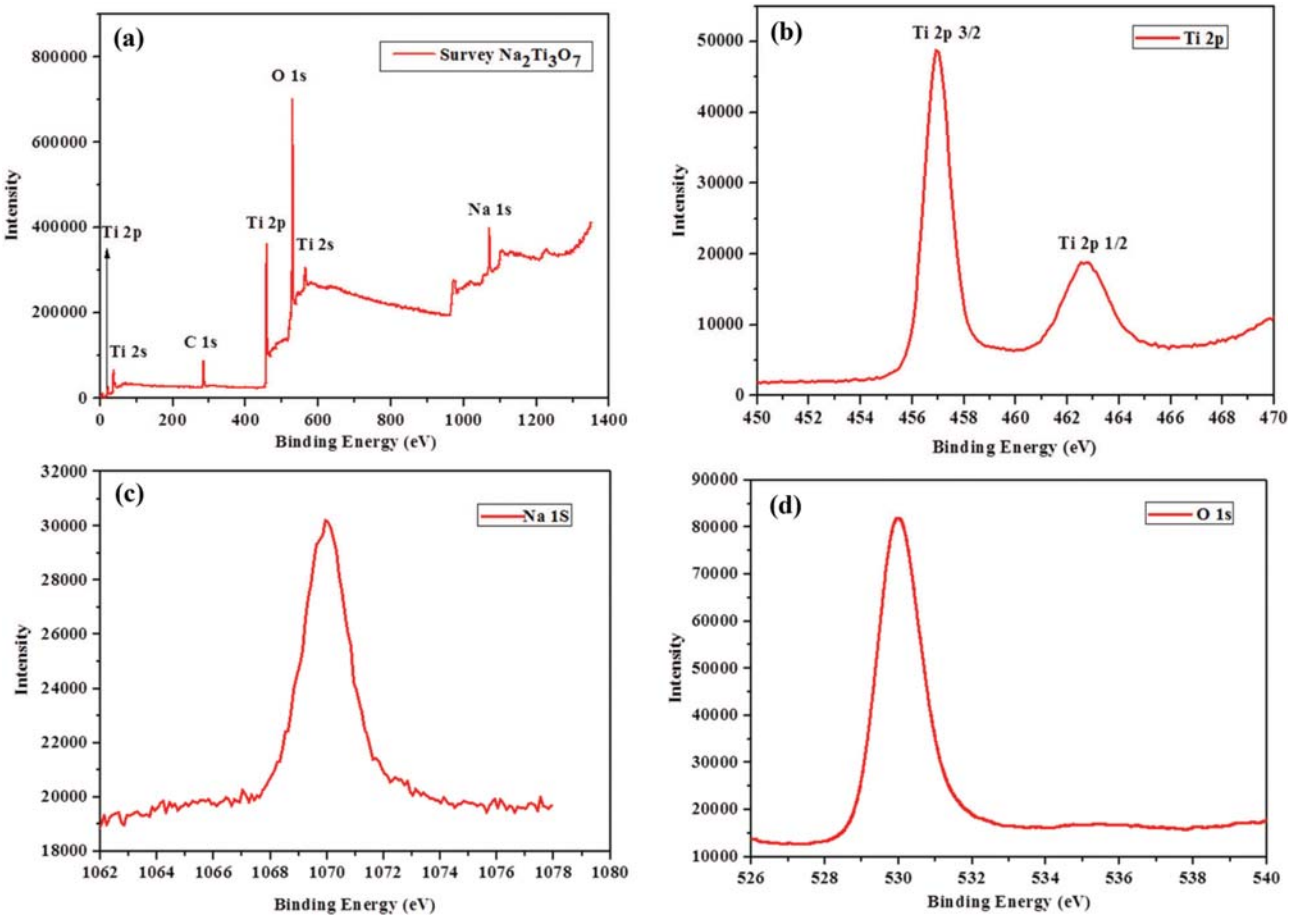

Fig. 3. High resolution X-ray photoelectron spectra (a) survey, (b) Ti, (c) Na and (d) O elements of as-prepared $Na_2Ti_3O_7$ nanotubes.

to be 227.4 m^2g^{-1}, which is higher than that reported [4,18]. The pore size distribution derived from the Barrett-Joyner-Halenda (BJH) approach is shown in the inset of Fig. 2(b). The pore volume and pore size of the mesopores are 0.281 cm^3g^{-1} and 3-10 nm, respectively. The moderately high specific surface area and mesoporous structure of the as-prepared $Na_2Ti_3O_7$ can provide more active sites for the HER.

The XPS survey spectrum of $Na_2Ti_3O_7$ is shown in Fig. 3(a). Fig. 3(b) shows the XPS results of Ti element, wherein two obvious peaks at 457 and 463 eV are attributed to Ti $2p_{3/2}$ and Ti $2p_{1/2}$, respectively [16]. The major peak at 1,070 eV (Fig. 3(c)) with the dominant Na signal is ascribed to Na^+, which are in correlation with the results of a previous report on $Na_2Ti_3O_7$ [4,17]. The intrinsic peak at approximately 530 eV (Fig. 3(d)) is ascribed to the Ti-O bond, which can be attributed to the +4 oxidation state of surface Ti.

The position of the optical band edge was estimated by UV-vis DRS, as shown in Fig. 4. The absorption wavelength of $Na_2Ti_3O_7$ was below 400 nm and has band gap energy of 3.25 eV (inset in Fig. 4), which is higher than that of the intrinsic band gap of P25 (3.1 eV) [19]. This implies that the as-prepared $Na_2Ti_3O_7$ could have an optical response in the shorter wavelength of UV-visible light due to its broader band positions in the UV region.

To enhance the photocatalysis process, three major factors are crucial: light absorption capability, adsorption of pollutant molecules, and fast charge transportation and separation [20]. Fig. 5(a) displays plot of UV absorbance with respect to different irradiation times for the degradation of RhB over 7.5 wt% $Na_2Ti_3O_7$ nanotubes. The characteristic absorption peak of RhB is observed at

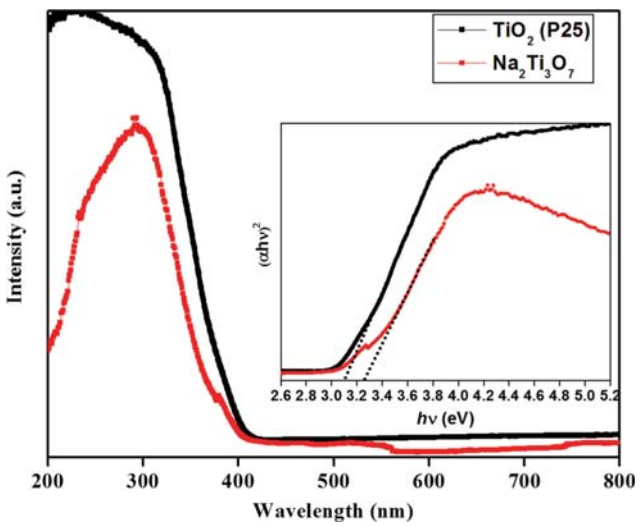

Fig. 4. UV-vis spectra, inset: Tauc plots of TiO_2 (P25) and as-prepared $Na_2Ti_3O_7$ nanotubes.

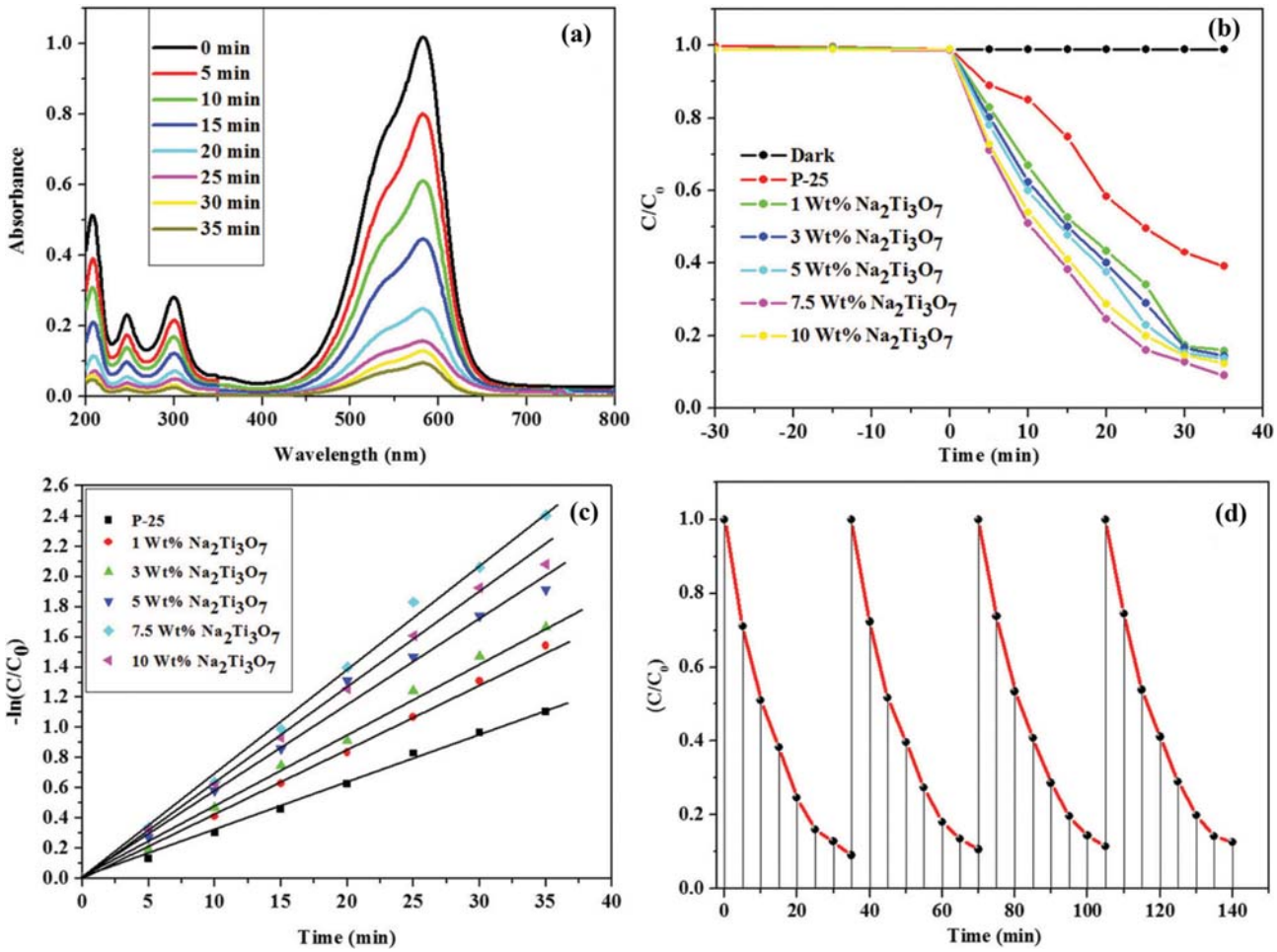

Fig. 5. (a) Time-dependent UV light absorbance spectra of the RhB solution along with 7.5 wt% $Na_2Ti_3O_7$ nanotubes taken at different times, (b) photocatalytic degradation activities of different photocatalysts, (c) the kinetic plot of photocatalytic degradation with various photocatalysts under UV light irradiation, and (d) recycling and reusability performance test of 7.5 wt% $Na_2Ti_3O_7$ nanotubes photocatalyst.

554 nm. Remarkably, after 35 min of UV light irradiation, 91% of RhB molecules had degraded with 7.5 wt% $Na_2Ti_3O_7$ nanotubes. The photocatalytic degradation of RhB over the P25 and different concentrations of $Na_2Ti_3O_7$ photocatalyst as function of time under UV light irradiation is shown in Fig. 5(b). Our photocatalytic studies demonstrated that after equilibrating in the dark for 30 min, most dye molecules (ca. 98%) remained in the solution with bare P25 as the catalyst. Notably, the improved photocatalytic performance of all $Na_2Ti_3O_7$ nanotube samples could be ascribed to their better light absorptivity than that of commercial P25 (Fig. 5(b)). With respect to the variation in the RhB concentration (C/C_0) with irradiation time, 91% of pollutant molecules could be eliminated by 7.5 wt% $Na_2Ti_3O_7$ nanotubes within 35 min. The decolorization of the RhB pollutant was obviously enhanced with the increasing concentration of $Na_2Ti_3O_7$ nanotubes in aqueous solution. The increase in the photocatalytic activity of the $Na_2Ti_3O_7$ nanotube catalyst is due to the presence of more active surface sites, which act as a sensitizer. However, within the same treatment intervals, the photocatalytic activity decreased to 87.6% in the presence of 10 wt% $Na_2Ti_3O_7$ nanotubes due to the agglomeration of individual nanotubes and covering the active sites with the higher amount of $Na_2Ti_3O_7$ nanotubes. The photodegradation efficiencies of RhB are in the order of 7.5 wt% $Na_2Ti_3O_7$>10 wt% $Na_2Ti_3O_7$>5 wt% $Na_2Ti_3O_7$ >3 wt% $Na_2Ti_3O_7$>1 wt% $Na_2Ti_3O_7$>P25. The photodegradation kinetics is adequately described by the equation $\ln(C_0/C)=-kt$, where k is the apparent rate constant, and C_0 and C are the initial and final concentration aqueous solution, respectively, as shown in Fig. 5(c). All samples followed a pseudo-first-order kinetics model. The 7.5 wt% $Na_2Ti_3O_7$ demonstrate the highest reaction rate constant ($k=0.0097\ min^{-1}$) which is 3.12 times higher than P25 ($k=0.0031\ min^{-1}$). Fig. 5(d) shows the recycling test results of 7.5 wt% $Na_2Ti_3O_7$ nanotubes photocatalyst followed by same photocatalytic test condition. Even after four cyclic tests, there was insignificant change in photoactivity and almost maintained the same photocatalytic performance from first till the fourth cycle end. Therefore, as-prepared $Na_2Ti_3O_7$ nanotubes could be applicable in practical use due to their beneficial features, including, inertness, high stability, low cost and ease of preparation.

Hydrogen production from water splitting in aqueous glycerol solutions over $Na_2Ti_3O_7$ catalysts under UV light and simulated solar light irradiation is shown in Fig. 6(a). The hydrogen production observed over $Na_2Ti_3O_7$ nanotubes under UV light (1,755

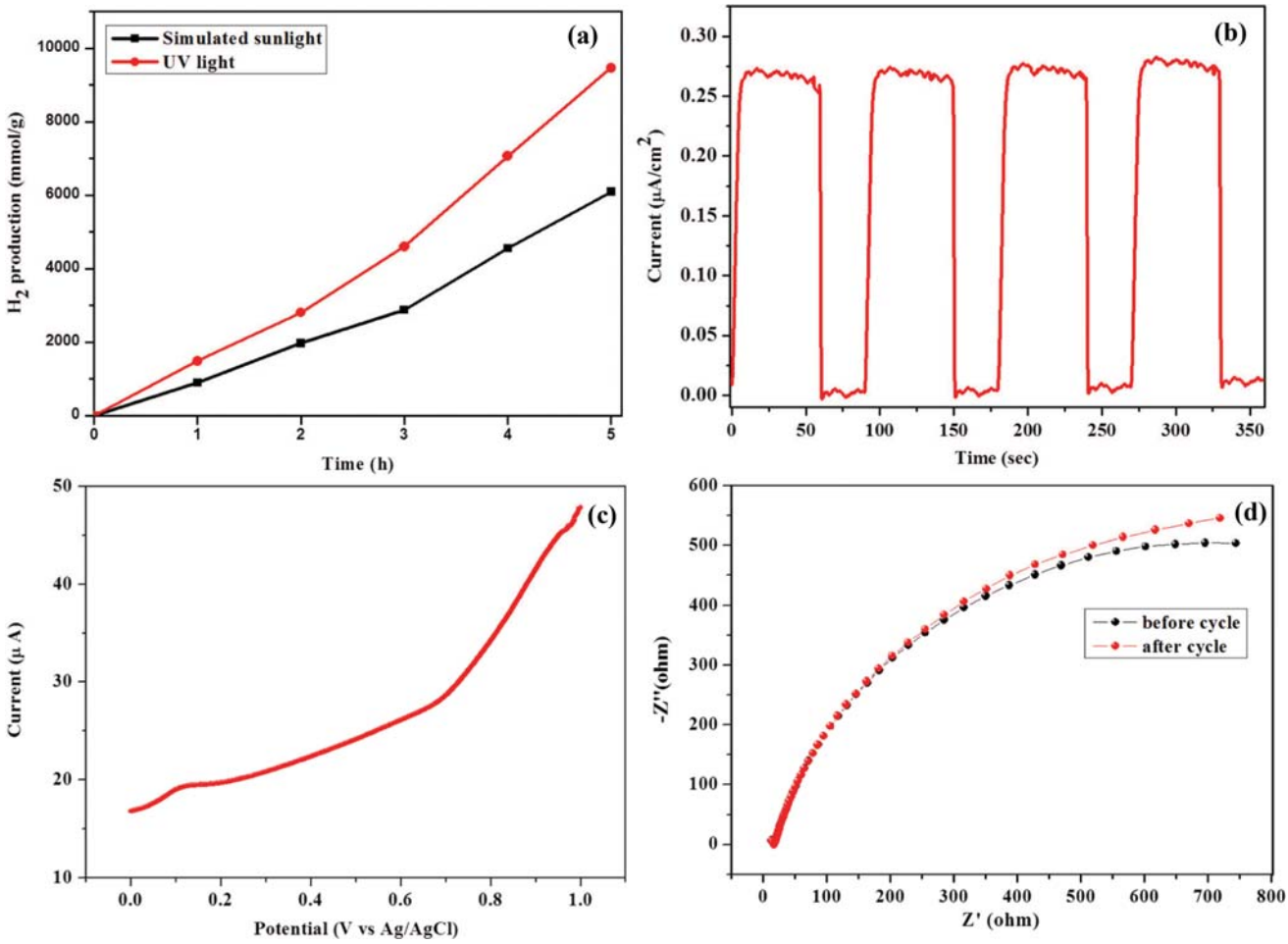

Fig. 6. (a) Photocatalytic H_2 evolution over $Na_2Ti_3O_7$ nanotubes in 5% glycerol: Water mixtures under UV and simulated solar light irradiation, (b) photocurrent responses of the PEC cells using $Na_2Ti_3O_7$ nanotubes as working electrode for four 60 s light-on-off cycles, (c) linear sweep voltammetry curve and (d) electrochemical impedance spectra of as-prepared $Na_2Ti_3O_7$ nanotubes.

$\mu mol \cdot g^{-1} \cdot h^{-1}$) is 1.55-fold higher than that of the simulated solar light irradiation (1,130 $\mu mol \cdot g^{-1} \cdot h^{-1}$) owing to more absorption in UV region. The optimal amount of catalyst lengthens the lifetime of the electron/hole pair, and the charge carriers are thus efficiently involved in redox reactions with adsorbed H^+ ions for the HER at the catalyst surface.

To explore the photocurrent of the $Na_2Ti_3O_7$ nanotubes, the photoelectrochemical (PEC) cell of $Na_2Ti_3O_7$ nanotubes and Na_2S (0.5 M) as electrolyte was employed under simulated solar light irradiation from xenon source (Max-300 lamp with an intensity of 40 $mW \cdot cm^{-2}$), and their amperometric I-t curve was acquired with four light on/off cycles within 60 seconds, as shown in Fig. 6(b). It is clear the photocurrent density of 0.27 $\mu A \cdot cm^{-2}$ at 0.4 V versus Ag/AgCl over $Na_2Ti_3O_7$ nanotubes. The photo-response of $Na_2Ti_3O_7$ nanotubes is attributed to significant photo-absorption, which is consistent with the optical result and promote the separation and transfer of photoinduced electrons and holes. The following reactions can explain the chemical conversion at the photochemical electrodes:

$$\text{At working electrode: } 2H_2O + 4h^+ \rightarrow O_2 + 4H^+ \quad (1)$$

$$\text{At counter electrode: } 4H^+ + 4e^- \rightarrow 2H_2 \quad (2)$$

To understand the importance of the electrochemical surface area effect of the $Na_2Ti_3O_7$ nanotubes, LSV and EIS were carried out. Fig. 6(c) shows the LSV curve of the $Na_2Ti_3O_7$ nanotubes. The results suggest that $Na_2Ti_3O_7$ nanotubes exhibit a much larger active surface area for the oxidation and reduction reactions and more active sites for the HER, which is consistent with the BET data. Furthermore, Nyquist plots of the $Na_2Ti_3O_7$ nanotubes before and after photocurrent test cycles are shown in Fig. 6(d). The reaction rate occurring on the electrode surface is exposed by the arc radius of the Nyquist plot. As result, the low, stable resistance demonstrates the benefit of the facile approach for $Na_2Ti_3O_7$ nanotube electrocatalysts. High photocatalytic performance with good stability towards the HER is very important for energy conversion systems. Remarkable electrochemical performance of $Na_2Ti_3O_7$ nanotubes is good evidence for pronounced charge transfer to enhance the photocatalytic H_2 production and degradation of pollutant.

To check the reproducibility of the results obtained for photocatalytic degradation of RhB dye and hydrogen production reactions over the $Na_2Ti_3O_7$ nanotubes, experiments were conducted

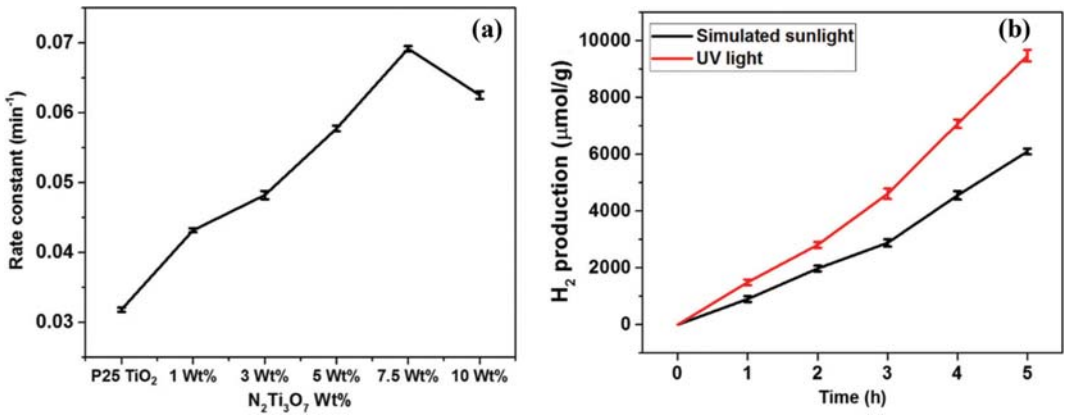

Fig. 7. Error bar graphs of the (a) RhB degradation and (b) H_2 production.

three times, and the corresponding error bar graphs are presented in the Fig. 7. The error bar graph of the rate constants obtained for the RhB degradation with commercial TiO_2 (P25) and different wt% of $Na_2Ti_3O_7$ nanotubes is displayed in Fig. 7(a). The standard deviation was calculated and found to be less than 2% for all the RhB degradation experiments. Similarly, the error bar graphs of the H_2 production under simulated solar light and UV light are presented in Fig. 7(b). The standard deviation for the hydrogen production experiments was less than 5%. This confirms that the degradation and H_2 production experiments are precise with good reproducibility.

CONCLUSIONS

$Na_2Ti_3O_7$ nanotubes were synthesized via a hydrothermal method and applied to the HER for the first time as an effective and highly stable catalyst for high-performance hydrogen evolution. Under optimum reaction conditions, such as glycerol concentration and catalyst amounts, 5 mg of catalyst under UV light can produce 1.55 times higher than that of simulated solar light irradiation. This result is mainly ascribed to the synergetic effect of the optimal amount of catalyst. Based on an economical view point as compared with graphene-based catalysts, $Na_2Ti_3O_7$ nanotubes are a more promising candidate as a low-cost catalyst for high-performance hydrogen evolution. Further, the obtained results are precise with good reproducibility.

ACKNOWLEDGEMENTS

This research was supported by the National Research Foundation of Korea (NRF) and funded by the Ministry of Science, ICT, and Future Planning (grant number 2017R1A2B1004860) and this work was also supported by the National Research Foundation of Korea (NRF) grant funded by the Korea government (No. NRF02017R1A4A1015581).

REFERENCES

1. H. Hayashi, T. Nakamura and T. Ebina, *J. Ceram. Soc. Jpn.*, **124**(1), 74 (2016).
2. A.-L. Sauvet, S. Baliteau, C. Lopez and P. Fabry, *J. Solid State Chem.*, **177**, 4508 (2004).
3. P. Umek, R. C. Korosec, B. Jancar, R. Dominko and D. Arcon, *J. Nanosci. Nanotechnol.*, **7**, 3502 (2007).
4. S. Preda, M. Rutar, P. Umek and M. Zaharescu, *Mater. Res. Bull.*, **71**, 98 (2015).
5. A. Rudola, N. Sharma and P. Balaya, *Electrochem. Commun.*, **61**, 10 (2015).
6. S. Anwer, Y. Huang, J. liu, J. Liu, M. Xu, Z. Wang, R. Chen, J. Zhang and F. Wu, ACS *Appl. Mater. Interfaces*, **9**(13), 11669 (2017).
7. Y.-T. Yu, *Korean J. Chem. Eng.*, **20**(5), 850 (2003).
8. D. J. D. Corcoran, D. P. Tunstall and J. T. S. Irvine, *Solid State Ionics*, **136-137**, 297 (2000).
9. S. Ogura, M. Kohno, K. Sato and Y. Inoue, *J. Mater. Chem.*, **8**, 2335 (1998).
10. Y. Wei, L. Shen, Z. Wang, W.-D. Yang and H. Liu, *Int. J. Hydrogen Energy*, **36**(8), 5088 (2011).
11. C.-Y. Xu, J. Wu, P. Zhang, S. P. Hu, J.-X. Cui, Z.-Q. Wang, Y.-D. Huang and L. Zhen, *Cryst. Eng. Commun.*, **15**, 3448 (2013).
12. H. Izawa, S. Kikkawa and M. Koizumi, *J. Phys. Chem.*, **86**, 5023 (1982).
13. Y. P. Zhang, L. Guo and S. H. Yang, *Chem. Commun.*, **50**, 14029 (2014).
14. T. Kasuga, M. Hiramatsu, A. Hosono, T. Sekino and K. Niihara, *Langmuir*, **14**, 3160 (1998).
15. Z. Zhang, J. B. M. Goodall, S. Brown, L. Karlsson, R. J. H. Clark, J. L. Hutchison, I. U. Rehman and J. A. Darr, *Dalton Trans.*, **39**, 711 (2010).
16. W. Wang, C. Yu, Z. Lin, J. Hou, H. Zhu and S. Jiao, *Nanoscale*, **5**, 594 (2013).
17. T. G. Deepak, D. Subash, G. S. Anjusree, K. R. Narendra Pai, S. V. Nair and A. Sreekumaran Nair, *ACS Sustainable Chem. Eng.*, **2**(12), 2772 (2014).
18. P. Sujaridworakun, S. Larpkiattaworn, S. Saleepalin and T. Wasanapiarnpong, *Adv. Powder Technol.*, **23**(6), 752 (2012).
19. V. Etacheri, C. D. Valentin, J. Schneider, D. Bahnemann and S. C. Pillai, *J. Photochem. Photobiol. C: Photochem. Rev.*, **25**, 1 (2015).
20. S. V. P. Vattikuti, C. Byon, Ch. V. Reddy and R. V. S. S. N. Ravikumar, *RSC Adv.*, **5**, 86675 (2015).